Synthesizer Stability Evaluation

E. N. Sosa and D. A. Tyner
Radio Frequency and Microwave Subsystems Section

An accurate and simple technique for measuring rms phase noise as a function of integration time for offset frequencies (10^{-3} Hz) close to the carrier is described. The accuracy of this method is verified by Allan Variance measurements in the time domain and through the use of Hadamard Variance for generating high-resolution spectral density measurements. Two different synthesizers are evaluated and the results are presented.

I. Introduction

Direct measurements of phase noise below 10 Hz from the carrier are not commonplace in industry. Special instrumentation and methods do exist for making close-in measurements well below 10 Hz, but these are costly as well as very time consuming. A recent need called for a simple but accurate technique that could be used by JPL and the synthesizer manufacturing industry. The need arose from a twofold requirement of the Phase 4 Receivers for VLBI. One aspect of the requirement called for cost-effective synthesizers because each receiver requires 12 synthesizers to provide a controlled selection of highly stable signals to be used for the second local oscillator signal. The other part of the requirement was related to an accurate in-house evaluation of close-in phase noise of a dozen potential candidate synthesizers. Thus, an accurate technique would assure the proper selection of the candidate synthesizer, and a simple test technique would be in keeping with lower cost units since this technique could be used for the acceptance testing of the production synthesizers. This report describes a method that is both accurate and amenable to production testing.

Typically, synthesizer manufacturers measure and state the stability of their units in terms of noise spectral density to within 10 Hz of the carrier. System requirements, on the other hand, are stated in user terms, for example, phase error as a function of sampling or integration time. The test method described below measures the synthesizer stability as phase error in the time domain. Allan Variance measurements (in the time domain) were used to verify the phase error measurements. In addition, the same Allan Variance measurements were transformed to the frequency domain and thus characterized the synthesizer's noise spectral density to within 10^{-3} Hz from the carrier. The accuracy of the transformed data was verified via high-resolution spectral density measurements using the Hadamard Variance. The sections below describe the various measurement techniques, the time domain to frequency domain transformations, and the range of applicability.

II. Frequency Domain

A. Noise Spectral Density

To specify stability, synthesizer manufacturers' data sheets typically specify $\mathscr{L}(f_m)$, the ratio of the single sideband power of phase noise in a 1-Hz bandwidth f_m Hertz away from the carrier frequency to the total signal power. The usual range for f_m is from 10 to 10^6 Hz, with no data relating to the

extremely close-in phase noise, which is of interest to those concerned with medium-to-long-term stability.

The customary method for generating $\mathscr{L}(f_m)$ curves utilizes spectrum analyzers, and the measurement techniques are straightforward and well-understood. To cover a wide range of f_m, several types of spectrum analyzers must be used and the typical measurement technique is shown in Fig. 1. The different configurations (A and B) displayed in Fig. 1 represent the method used to compensate for the limited offset range capability of typical spectrum analyzers. The newest generation of spectrum analyzers, like the HP 8568, provide most of the required range from offsets of 80 Hz to greater than 1 MHz away from the carrier, at the actual carrier frequency (Configuration A: f_o = 100 MHz). Older analyzer models require more overlap with lower offset frequency domain analyzers such as the HP 3581 Wave Analyzer (max $f_o < 50$ kHz) or the HP 3585 low-frequency spectrum analyzer ($f_o < 40$ MHz. These instruments measure $f_m > 3$ Hz and 25 Hz respectively, but require the measurement setup of configuration B, which adds an external mixer prior to the low-frequency spectrum analyzer, and thus extends its upper-frequency limit. These techniques provide a direct measure of the noise power at different offset frequencies, and require the corrections delineated in the Appendix to derive the SSB noise in 1 Hz. Configurations A and B were used to generate the $\mathscr{L}(f_m)$ curve depicted in Fig. 2 for the laboratory model synthesizer built by JPL, similar in design to the Mark III-Haystack Digitally Controlled Synthesizer (DCS). Spectral densities generated with the different instruments agree well where data overlap existed, and furthermore, data connect smoothly between different regions where measurements were not taken. The accuracy of the spectral density measurements is estimated to be within ±3 dB. The other $\mathscr{L}(f_m)$ curve, also in Fig. 2, was obtained from the data sheet of a commercially available synthesizer. Both of these curves illustrate the frequency range that can be normally covered, but which does not get into the close-in range.

To extend the noise spectral density curves into the extremely close-in range, use was made of the Allan Variance method. Medium-to-long term stability performance in the time domain can be practically and meaningfully measured by fractional-frequency deviations (the square root of Allan Variance). The testing requires a statistical evaluation of the sampled synthesizer frequency, as it deviates from a reference standard. In general, fractional-frequency deviation does not provide a precise estimate of spectral density for offsets, f_m, far away from the carrier. However, for close-in phase noise, sufficient accuracy is obtainable, as shown later by the direct rms phase jitter measurements. Fractional-frequency deviation data were obtained for the two synthesizers whose noise spectral densities are given in Fig. 2. The measurement technique is illustrated by the block diagram in Fig. 3, with the HP 5390 Frequency Stability Analyzer shown used to sample the beat note between the reference and synthesizer under test and to calculate the fractional-frequency deviation, $\sigma_y(\tau)$. Narrow noise bandwidths (f_h), corresponding to small beat notes (ν_b), were needed for measurement of close-in spectral density components of the continuous noise distributions. A wider f_h measurement is described in a later section to supplement this close-in data base with the middle to far-out offset frequency components. The measured stability performance for the two synthesizers is depicted in Fig. 4 for ν_b = 1 Hz. Medium-to-long-term stability performance is covered by the integration times, τ, from 10 to 10^3 seconds. Different noise processes in the synthesizers give rise to the slopes of the fractional-frequency deviation, $\sigma_y(\tau)$ plots in Fig. 4. The noise process can be identified by its slope, and, by knowing the noise process, a time-to-frequency transformation can be made thus translating the accurate long-term stability measurements into close-in noise spectral density data.

B. Time-to-Frequency Transformations

Transformations from the time domain to the frequency domain have been described (Refs. 1 and 2), and have been applied by Sward (Ref. 3) to the highly stable hydrogen maser over the same offset frequency range of interest (10^{-3} to 10^6 Hz). A method similar to Sward's was used in this evaluation except that more exact formuli (Ref. 4) were used here for calculating the f_m corresponding to a particular integration time τ. A simple reciprocal conversion can lead to up to an order of magnitude error from the exact value. The more exact method involves calculating the f_m at the intersection points where the dominant noise process changes and gives rise to a different slope. For example, in Fig. 4 the $\sigma_y(\tau)$ plot for the commercial synthesizer shows a break point (a change in slope) at τ = 40 s. The simple reciprocal conversion leads to f_m = 0.025 Hz, while the more exact formula results in f_m = 0.007 Hz.

The extension of the noise spectral density plots were generated by approximating the experimental $\sigma_y(\tau)$ data with slopes corresponding to well-known noise processes. In the plots of Fig. 4, both units were considered to be composed of two noise processes. The commercial unit consisted of white frequency (slope = −1/2) and random walk frequency (+1/2), while the JPL-built unit exhibited flicker phase (slope = −1) and white frequency (−1/2).

The transformations used for the 3 different noise processes are

$$\mathscr{L}(f_m) = \frac{(\sigma_y(\tau) f_o \tau 2.565)^2}{2.184 + \ln(f_h \tau)} f_m^{-1} \qquad \text{flicker phase} \qquad (1)$$

$$\mathscr{L}(f_m) = (\sigma_y(\tau) f_o \tau^{1/2})^2 f_m^{-2} \quad \text{white frequency} \quad (2)$$

$$\mathscr{L}(f_m) = (\sigma_y(\tau) f_o \tau^{-1/2}\, 0.276)^2 f_m^{-4} \text{ random walk frequency} \quad (3)$$

in which f_o denotes the carrier frequency and f_h is the measurement bandwidth. The exact values for f_m were found by solving simultaneously for f_m and τ with pairs of the above equations whose corresponding noise processes intersect. The τ at the intersection point is known from the experimental fractional-frequency deviation data and the corresponding f_m is determined.

The transformed time domain data are shown plotted in Fig. 5 as extensions of the noise spectral density plots previously discussed. The transformed $\sigma_y(\tau)$ data "lines-up" well with the measured $\mathscr{L}(f_m)$ curves. However, to ascertain the accuracy of the transformations, close-in phase noise spectral density measurements were made with the HP5390 Frequency Stability Analyzer as configured in Fig. 3. This instrument also makes use of the Hadamard Variance, which was developed for making high-resolution spectral analysis. Frequency domain data is calculated from the time domain data provided by digital counters. The data obtained with the HP5390 is also plotted in Fig. 5, and support the simpler transformations used above.

III. Phase Noise in the Time Domain

It was previously mentioned that from a system's point of view, the desired stability parameter is phase noise in the time domain. In this section several techniques are described to measure phase noise or jitter as a function of integration time with conventional instrumentation. Also described below are how these measurements compare to the stability measured via the fractional-frequency deviation technique. Direct calorimetric phase jitter measurements were made and these were compared with the corresponding transformed $\sigma_y(\tau)$ measurements. Good agreement was obtained. Additional phase error data as a function of time was obtained by measuring temperature stability of several synthesizers. A further use of the phase jitter data involves the calculation of the relative power between noise and carrier in order to supply another frequency domain representation of synthesizer stability.

Using readily available instrumentation, a method was developed to measure phase error at selected integration times. The measurement block diagram for calorimetric true rms phase jitter is shown in Fig. 6. The technique involves heterodyning the phase noise spectra to baseband and calibrating the phase fluctuations to the measured rms voltage (Ref. 5). To generate phase jitter data as a function of integration time, it was necessary to alternate true rms detectors. Each detector had a different (99%) response time and, with six detectors, integration times from 60 ms to 45 s were covered in six points. The integration time span is due to several different implementations of a true rms converter, utilized in the calorimetric detectors listed in Fig. 6. The shorter taus are obtained in high-speed monolithic circuits that can effectively integrate the high peak-to-rms-noise voltages into their equivalent root mean square values. Longer sampling times require more massive heat generating and detecting hardware and usually operate over much larger bandwidths. Sensitivity also degrades substantially for the longest τ detector (45 s) requiring a larger gain to measure the equivalent rms phase jitter (a dynamic range constraint for high spectral purity signal measurement).

Phase jitter is calculated from the measured raw noise and sinusoidal voltages by

$$\Delta\phi_{rms}(\tau) = \frac{(57.296 \text{ deg/rad})}{\sqrt{2}} \frac{V_{noise}}{V_{beat}} \quad (4)$$

where $\Delta\phi_{rms}(\tau)$ is the rms jitter in degrees of a synthesizer at f_o, τ is the 99% response time of digital voltmeter (DVM), V_{noise} is the true rms voltage of the noise fluctuations, and V_{beat} is the true rms voltage of the calibration beat note. This assumes that the reference synthesizer is 10 dB more stable than the synthesizer under test. If the synthesizers are nearly the same, another $1\sqrt{2}$ factor must be added to ascertain the individual synthesizer performance. The data obtained for the two synthesizers are plotted in Fig. 7 for a carrier frequency of 100 MHz.

The JPL-built synthesizer exhibited between 0.7 and 1.0 degrees rms of jitter for $\tau \leqslant 45$ s at 100 MHz. With the same setup, in the short integration times the commercial synthesizer manifested a hundredfold lower noise, but also drifted relatively more in the longer integration times. The fourfold degradation at $\tau = 45$ s, compared to the jitter for $\tau \leqslant 2$ s, demonstrates the type of phase drifts that can occur in some synthesizers, probably due to environmental factors.

It is interesting to note the nearly flat phase jitter slope at the low taus, for all of the curves depicted in Fig. 7. The dashed lines connecting the open symbols represent the corresponding phase jitter values obtained by applying a simple transformation of the $\sigma_y(\tau)$ data given for both synthesizers in Fig. 8. These fractional-frequency deviations, measured with ν_b = 10 kHz and in a 25-kHz bandwidth (f_h), offer an excellent methodology comparison to the calorimetric data where f_h = 15 kHz. The transformation converts $\sigma_y(\tau)$ vs

τ to $\Delta\phi_{rms}$ vs τ by a straightforward scaling of the $\Delta f/f_o$ values. The equation used,

$$\Delta\phi_{rms}(\tau) = \sigma_y(\tau) \cdot f_o \cdot \tau \cdot 360 \qquad (5)$$

also clarifies the observed short-term $1/\tau$ relation of the $\sigma_y(\tau)$ data and the independently measured constant $\Delta\phi_{rms}$ slope. Obviously as τ increases, the $\sigma_y(\tau)$ values must decrease equally in proportion to maintain a constant phase jitter slope. Thus a $1/\tau$ fractional-frequency deviation slope translates into a constant phase jitter. Furthermore, as the phase errors become larger for longer sampling times, the $\sigma_y(\tau)$ curves must flatten out and then eventually turn upward, typically beyond $\tau \cong 1000$ s (as observed in Fig. 8).

Equation 5 can also be applied to the $\sigma_y(\tau)$ data shown in Fig. 4, but due to the much smaller measurement bandwidth (f_h = 1 Hz) and ν_b = 1.0 Hz, no meaningful relation exists to the measured calorimetric jitter taken in a 15-kHz bandwidth. The $\sigma_y(\tau)$ values of Fig. 4 would essentially relate to only the close-in noise spectral density as previously demonstrated, and thus exclude the predominant noise pedestal of the JPL-built DCS at offset frequencies between 0.1 and 10 kHz away from the carrier. An indication of this is found by comparing the $\sigma_y(\tau)$ values of Figs. 4 and 8, at τ = 1 s. The JPL-built DCS suffers a 42-fold loss in stability, while the commercial unit degrades by only a factor of 3, for the increased measurement bandwidth from 1 Hz to 25 kHz, thus showing the importance of measurement bandwidth. Corroboration of the time and frequency domain data is enhanced by the observed downward trend of the transformed $\Delta\phi_{rms}$ of Fig. 7, for the short integration times of the commercial synthesizer. This type of behavior is expected due to the observed rapid drop in noise spectral density, for $f_m \geqslant 100$ Hz found in Fig. 5.

The empirical data base established to generate the curves of Fig. 7 can also be used directly in the frequency domain, to generate another set of spectral densities. This is because the calorimetric method is basically a hybrid of the conventional $\mathscr{L}(f_m)$ measurement scheme and several variable τ detectors. The formula to generate $\mathscr{L}(f_m)$ is:

$$\mathscr{L}(f_m) = 20\log\left(\frac{V_{noise}}{\sqrt{2}\,V_{beat}}\right) - 10\log(f_h) - 3\ \text{dB} \qquad (6)$$

where V_{noise} is the true rms voltage at offset f_m Hz from f_o, V_{beat} is the true rms voltage of the $\nu_b = f_m$ beat note, f_m is the wave analyzer's tuned frequency, f_h is the noise bandwidth, and the (−6 dB or −3 dB) factor is for SSB noise with equivalent sources or for a reference with 10-dB lower noise.

This measurement also utilizes the test configuration in Fig. 6 (see Ref. 6), and in Table 1 typical phase jitter is listed for each synthesizer tested and their related calculated spectral densities. The offset frequency, f_m, in this case was a distributed parameter due to the wideband low-pass filter used (Fig. 6: f_h = 15 kHz) and thus the calculated value represents an integration of the noise sidebands normalized to a 1-Hz bandwidth without a specific f_m (i.e., DC $< f_m <$ 15 kHz). Even so, the calculated results match well with the measured $\mathscr{L}(f_m)$ displayed in Table 1 or in Fig. 5. Additional jitter data were taken as a function of f_m by utilizing the wave analyzer as a variable tuned filter, as shown beneath the dotted line in Fig. 6. Results taken in this manner demonstrated the relationship of wider resolution bandwidths and variable offset frequency f_m, and confirmed the curves of Fig. 2. It is thus practical to measure spectral densities of noise sidebands by the apparatus used to measure phase jitter as a function of integration time.

IV. Temperature Stability

Phase stability as a function of time also becomes temperature related, due to the susceptibility of synthesizers to environmental changes. The temperature coefficient of output phase was measured and can be related to long-term phase instabilities. The measurement block diagram used is found in Fig. 9. The data were taken by applying a temperature step (ΔT = 20°C) to the synthesizers under test and watching their phase change with respect to the reference synthesizer, at ambient (Ref. 7). An exponential phase response resulted from the applied step temperature change, and the phase stabilized at a new value after 20 or 30 min. By dividing the phase step by the temperature step, one arrives at a number that indicates the susceptibility of phase changes in the expected receiver environment. The equation is simply

$$\frac{\Delta\phi}{\Delta T} = \frac{\phi_{init}(T = T_1) - \phi_{final}(T = T_2)}{T_2 - T_1} \qquad (7)$$

where $\Delta\phi/\Delta T$ is the change in output phase per degree centigrade change in temperature, ϕ_{init} and ϕ_{final} are steady-state values displayed on the vector voltmeter before and after the applied thermal step $\Delta T = T_2 - T_1$.

Results of this test are tabulated in Table 2 for each synthesizer and these data indicate that a synthesizer such as the JPL-built DCS, with a lower parts count, is about 5 times less sensitive to environmental variations than the commercial unit tested.

Another attribute of the temperature stability measurement scheme is the ability to generate a frequency stability value,

$\Delta f/f_o$, for the equivalent thermal time constant of the synthesizer tested. The same exponential phase vs time curve discussed above is used to calculate the $\Delta f/f_o$ (τ_{therm}). The $1/e$ (or 63% of the final phase value) time interval, and the actual $\Delta\phi$, has been normalized to the operation frequency and recorded in Table 2. These numbers represent nonstatistical phase drift susceptibilities found at longer integration times ($\tau > 1$ min), and thus further buttress the long-term stability analysis. The expression used to compute the temperature stability displayed in Table 2 and Fig. 8 is

$$\frac{\Delta f}{f_0}(\tau_{therm}) = \frac{\phi_{init}\ (t=0) - \phi_{63\%}\ (t=\tau_{therm})}{360 \cdot \tau_{therm} \cdot f_o} \qquad (7)$$

where ϕ_{init} $(t = 0)$ is the initial steady phase, prior to applied step ΔT, $\phi_{63\%}$ $(t = \tau_{therm})$ is the phase shift incurred after τ_{therm} seconds, and τ_{therm} is 63% or ϕ_{final} $(t \geq 3\,\tau_{therm})$ measured in seconds.

The long-term σ_y (τ) values seem to connect fairly well to these indirectly generated $\Delta f/f_0$'s as the expected up turn in the two curves occurs at their respective thermal time constants.

V. Conclusion

In the absence of conventional instrumentation for measuring close-in noise, a method has been developed that not only utilizes readily available equipment, but that can be used for production testing. The measurement technique utilizes the different time constants inherent in the different types of true rms meters. Two different synthesizers were measured, and the results were in very good agreement with stability data obtained by more sophisticated methods and instruments. Allan Variance was used to establish that, via transforms, fractional-frequency deviations gave a good representation of close-in phase noise. This was also supported by spectral density measurements using the HP5390 Frequency Stability Analyzer. Allan Variance measurements were subsequently transformed to phase noise as a function of time and compared to the phase jitter measurements made by the method herein described. Good agreement was obtained up to $\tau \doteq 45$ seconds, which corresponds to 6×10^{-3} Hz. Knowledge of the noise process for the particular synthesizer determines the slope beyond 45 seconds. More accurate determination of $\Delta\phi_{rms}(\tau)$ beyond 45 seconds can still be accomplished by $\sigma_y(\tau)$ measurements except that these take longer test time. Other production-oriented measurement techniques that offer potential are digital spectrum analyzers that utilize the FFT (Fast Fourier Transform) to transform time domain samples in parallel into the frequency domain with a minimal delay, or a new class of (digital) video chart recorders that can provide statistical averaging of the phase drifts as a function of integration time. A few major synthesizer vendors currently utilize the HP 3582 FFT Spectrum Analyzer for their production testing of close-in ($f_m > 1$ Hz) noise spectral densities for their top line, low-noise synthesizers. The instrumentation just mentioned is capable of measuring considerably closer to the carrier, within 10^{-2} Hz, but little need typically has been expressed for such information. It turns out that VLBI receivers also require measurements of phase error as a function of integration time, and any frequency domain method would necessitate accurate transformations from the frequency to the time domain to assure compliance with the overall system design.

While the results of the measurement techniques herein described agreed well with transformed data, the overall limits of applicability were not established. Evidently the measurement technique is valid for the case of synthesizers locked to a spectrally pure hydrogen reference source, and for the integration times applied. Further investigation into the nonstationary (random walk) noise phenomenon may establish limits to the application, and may offer the optimal method of measuring long-term instabilities of phase.

References

1. Scherer, D., "Design Principles and Test Methods for Low Phase Noise RF and Microwave Sources," Hewlett-Packard RF and Microwave Measurement Symposium and Exhibition, June 23-24, 1980 (an update to his earlier report in *Microwaves*, pp. 113-122, April and May 1979).

2. Rutman, J., "Characterization of Phase and Frequency Instabilities in Precision Frequency Sources: Fifteen Years of Progress," *Proc. of IEEE*, Vol. 66, No. 9, pp. 1048-1075, Sept. 1978.

3. Sward, A., "Measurement of the Power Spectral Density of Phase of the Hydrogen Maser," *Quarterly Technical Review*, Vol. 1, No. 4, pp. 30-33, Jet Propulsion Laboratory, Pasadena, Ca., Jan. 1972.

4. Burgoon, R., and Fisher, M. C., "Conversion Between Time & Frequency Domain of Intersection Points of Slopes of Various Noise Processes," *32nd Annual Frequency Control Symposium Proceedings*, National Technical Information Service, pp. 514-519, 1978.

5. Walls, F. L., Stein, S. R., Gray, E., and Glaze, D. J., "Design Consideration in State-of-the-Art Signal Processing and Phase Noise Measurement Systems," *30th Annual Frequency Control Symposium Proceedings*, National Technical Information Service, pp. 269-274, 1976.

6. Fischer, M. C., "Frequency Domain Measurement Systems," *10th Precision Time and Time Interval Applications and Planning Meeting Proceedings*, December 1978. Technical Information & Administrative Support Division, Goddard Space Flight Center, Greenbelt, Md. (Also available in *Microwaves*, July 1979, pp. 66-75, entitled: "Analyze Noise Spectrum With Tailored Test Gear").

7. MacConnell, J., and Meyer, R., "L-Band Frequency Multipliers: Phase Noise Stability and Group Delay," *Deep Space Network Progress Report, TR 32-1526*, Vol. X, pp. 104-109, Jet Propulsion Laboratory, Pasadena, Ca., Aug. 1972.

Table 1. Calculated average noise spectral density derived from phase jitter data

Synthesizer Model	Actual $\Delta\phi$ rms, deg rms	Calculated $\mathscr{L}(f_m)$[a] dBc/Hz	Measured $\mathscr{L}$(100 Hz), dBc/Hz
JPL-built DCS	0.81	−82	−75
Commercial unit	0.0083	−122	−131

[a] f_m, the offset frequency, is now a distributed parameter, somewhere between 1 and 15,000 Hz.

Table 2. Temperature coefficient of output phase and frequency deviation test results

Synthesizer	$\Delta\phi$/°C, deg peak/°C	$\Delta f/f_o$ (τ_{therm})	τ_{therm}, s
JPL-built DCS (variation of 3)	2.2 ± 1	$(5.6 \pm 4) \times 10^{-13}$	720 ± 300
Commerical unit	10.2 ± 1	5.1×10^{-13}	3000 ± 100

CONFIGURATION A

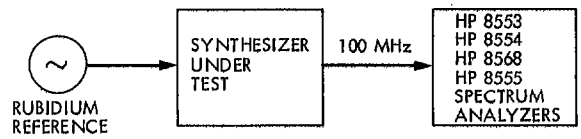

CONFIGURATION B

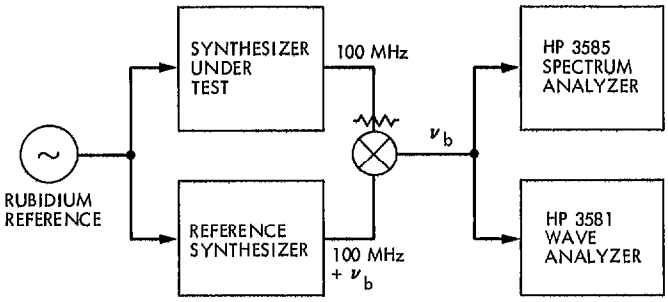

KEY PARAMETERS

ANALOG SPECTRUM ANALYZERS	MIN OFFSET[a] f_m, Hz	CONFIGURATION
HP 8568	80	A
HP 8555	800	A
HP 8554	800	A
HP 8553	100	A
HP 3585	25	B
WAVE ANALYZER[b]		
HP 3581	3.0	B

[a] WHERE $\mathcal{L}(f_m) < -80$ dBc/Hz AND $\nu_b = f_m$

[b] MAX OFFSET LIMITED HERE TO $f_m \leq 50$ kHz

Fig. 1. Noise spectral density, $\mathcal{L}(f_m)$, measurement block diagram

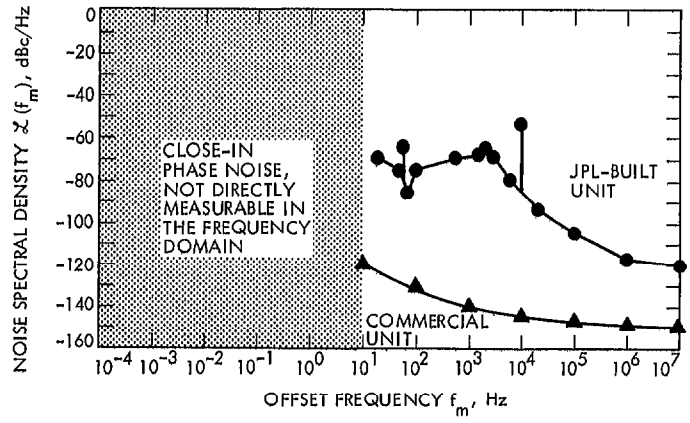

Fig. 2. Measured SSB phase noise of JPL-built DCS and commercial unit

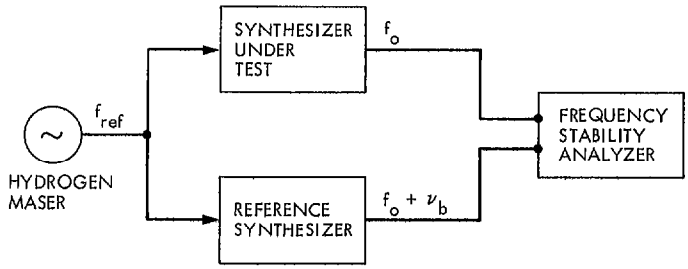

KEY PARAMETERS

FREQUENCY STABILITY ANALYZER	HP 5390
$\sigma_y(\tau)$ (TIME DOMAIN)	
BEAT NOTE AND NOISE BANDWIDTH (f_h)	
ν_b = 1.0 Hz	f_h = 1.0 Hz
ν_b = 10 kHz	f_h = 25 kHz
REFERENCE SYNTHESIZER	
HP 8662 (OR)	$f_o = 100 + \nu_b$ MHz
HYDROGEN MASER	f_o = 100 MHz
EXTERNAL REFERENCE	
HYDROGEN MASER	f_{ref} = 5 MHz
NUMBER OF SAMPLES	$n \geq 25$
SYNTHESIZER UNDER TEST	
JPL-BUILT DCS	f_o = 100 MHz
COMMERCIAL UNIT	f_o = 100 MHz
TYPICAL NOISE FLOOR	$\sigma_y(1s) < 1 \times 10^{-14}$

Fig. 3. Fractional frequency deviation measurement block diagram

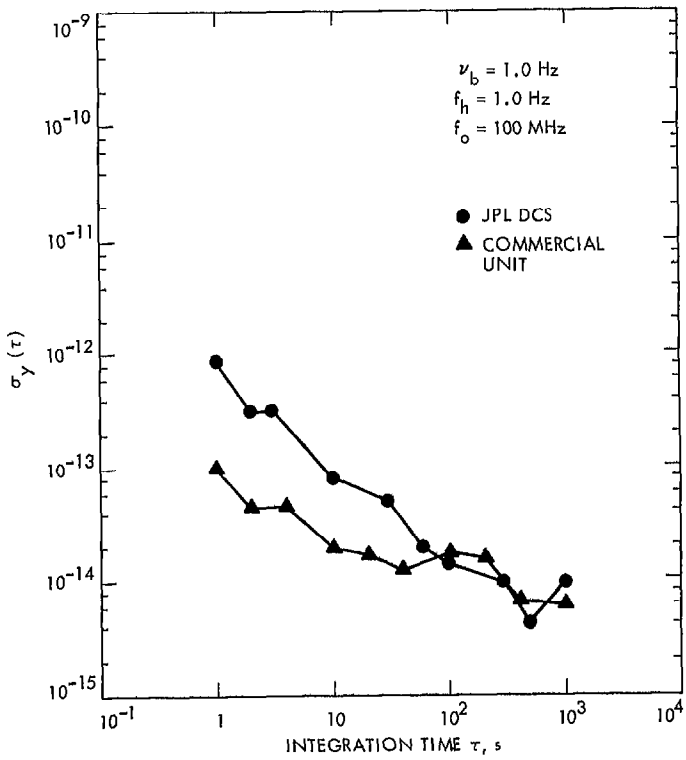

Fig. 4. Fractional frequency deviation of JPL-built DCS and commercial unit

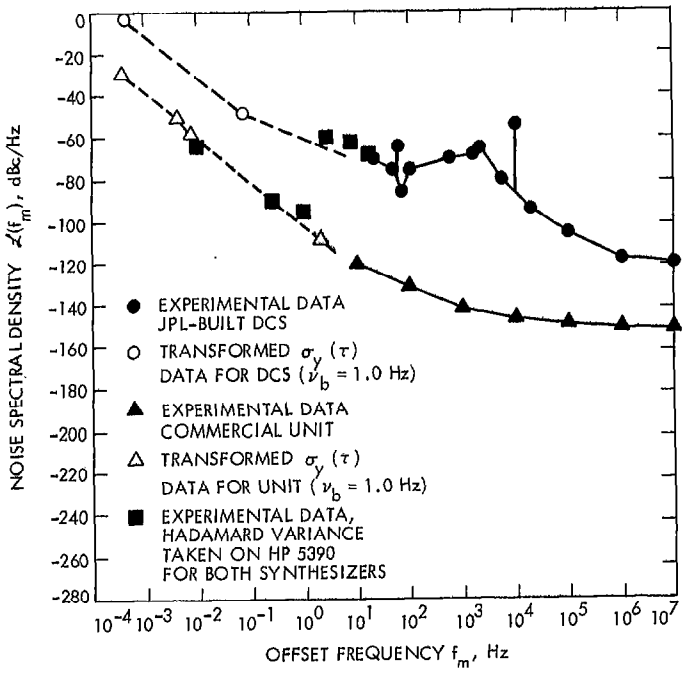

Fig. 5. Composite noise spectral density

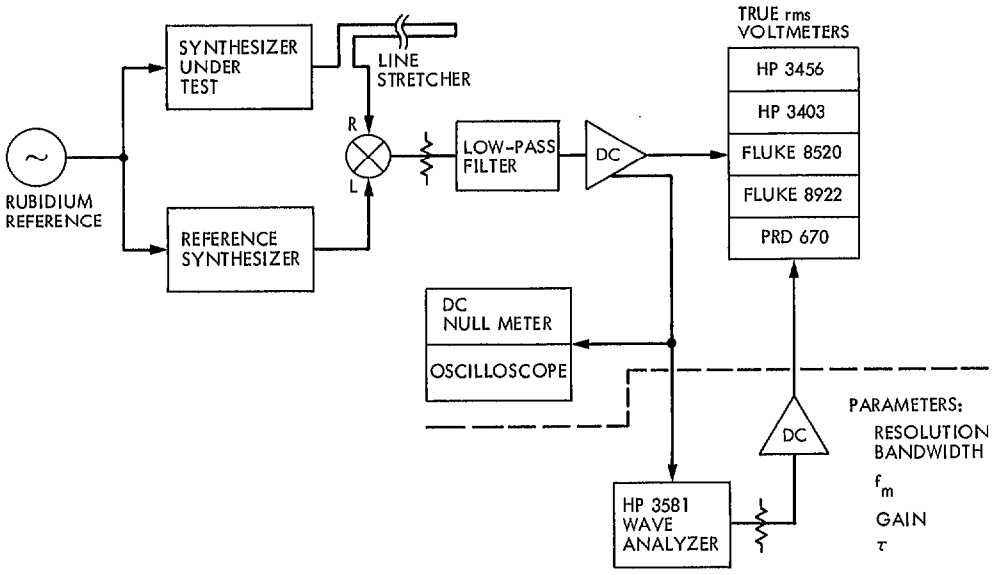

KEY PARAMETERS

TRUE rms VOLTMETER INTEGRATION TIMES (τ)	
HP 3456	0.06 s
FLUKE 8520	0.10 s
HP 3403 (FAST/SLOW)	1.0/10 s
FLUKE 8922 (FAST/SLOW)	2.0/7 s
PRD 670 (DC RESPONDING)	45.0 s
MEASUREMENT BANDWIDTH	
DYNAMICS 6050 DC AMP	DC TO 15 kHz
WAVE ANALYZER (HP 3581)	
$\Delta\phi_{rms}$ vs BW	3 Hz ≤ RES BW ≤ 300 Hz
$\Delta\phi_{rms}$ vs f_m	50 Hz ≤ f_m ≤ 5 kHz
TYPICAL NOISE FLOOR	
$\mathcal{L}$ (1 kHz) < -130 dBc/Hz	
$\Delta\phi_{rms}$ < 0.001 deg rms (in 15 kHz)	

Fig. 6. Calorimetric phase jitter vs τ measurement block diagram

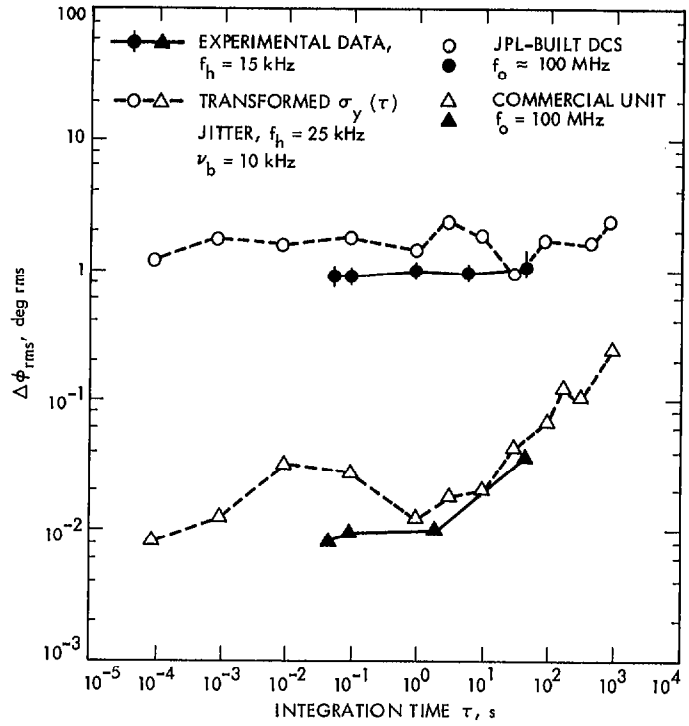

Fig. 7. Rms phase jitter vs τ of JPL-built DCS and commercial unit

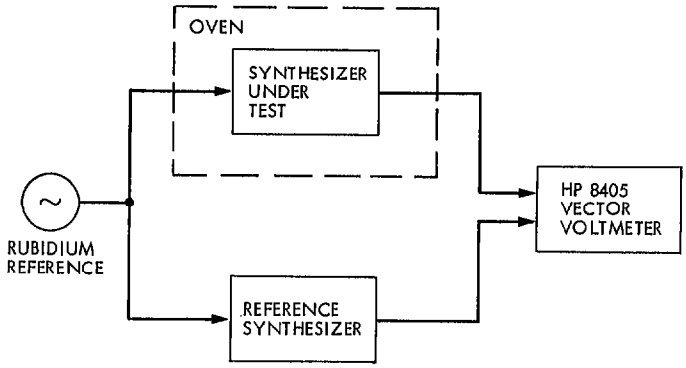

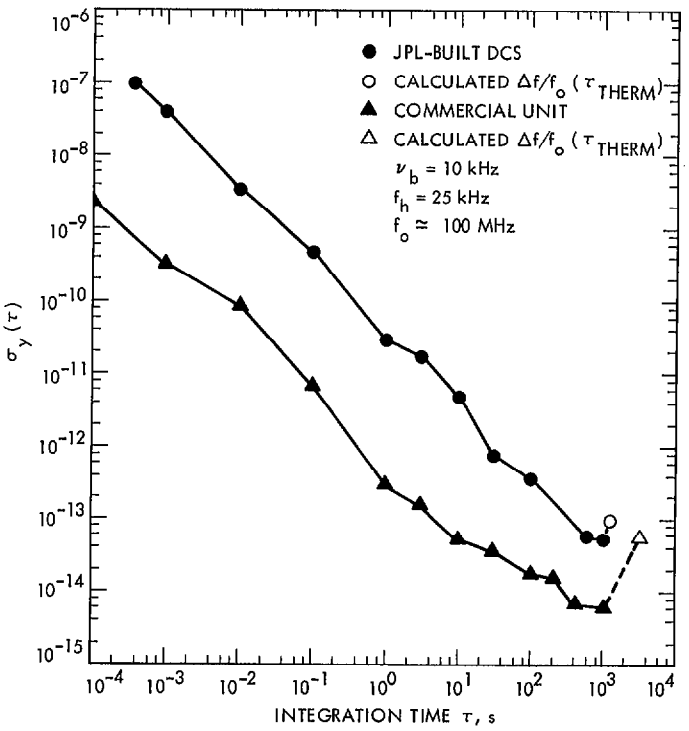

Fig. 8. Fractional frequency deviation of commercial unit and of JPL-built DCS

KEY PARAMETERS

PHASE SHIFT RESOLUTION	0.1 deg UP TO 1 GHz
PHASE SHIFT ACCURACY	± 1.5 deg
TEMPERATURE ACCURACY	± 0.2°C
TEMPERATURE STEP, ΔT	20°C
TYPICAL NOISE FLOOR	
TEMPERATURE COEFFICIENT OF OUTPUT PHASE	< 0.05 deg/°C
$\Delta f/f_o$ (WHERE: f = 100 MHz, $\tau \approx 60$ s)	$< 1 \times 10^{-14}$

Fig. 9. Temperature coefficient of output phase measurement block diagram

Appendix

Power Spectral Density Calculations

I. Spectrum Analyzer (Fig. 1)

$$\mathscr{L}(f_m) = -(P_{carrier} - (P_{noise} - 6\text{ dB} + 2.5\text{ dB} - 10\log(f_h) - 3\text{ dB}))$$

where:

$\mathscr{L}(f_m)$ is in dBc/Hz; or dB below f_o the carrier, measured at the offset f_m, in 1-Hz equivalent noise bandwidth

$P_{carrier}, P_{noise}$ are measured powers in dBm

−6 dB is a factor for SSB and the displayed carrier power in rms, rather than peak power

+2.5 dB corrects for log amp at IF

f_h is noise bandwidth; ≅ 1.15 X resolution BW

(−3 dB or −0 dB) is for two equivalent sources or if reference is 10-dB lower noise

II. Wave Analyzer (Fig. 1, Configuration B; Fig. 6)

$$\mathscr{L}(f_m) = -(P_{carrier} - (P_{noise} - 6\text{ dB} + 1.05\text{ dB} - 10\log(f_h) - 3\text{ dB}))$$

where:

+1.05 dB is the correction factor for white noise as average responsing detector is calibrated to read true rms, for a discrete signal

f_h is equivalent noise bandwidth; ≅ 1.10 X resolution BW, as typical wave analyzers utilize narrower IF filters